



Research article

Integrating network analysis and experimental validation to reveal the mechanism of si-jun-zi decoction in the treatment of renal fibrosis

Xinxin Yu¹, Xing Pu¹, Yu Xi¹, Xiang Li, Wei Jiang, Xiaoling Chen, Yong Xu, Juan Xie, Hailun Li^{**}, Donghui Zheng^{*}

Department of Nephrology, Affiliated Huai'an Hospital of Xuzhou Medical University, Huai'an, Jiangsu, 223002, PR China

ARTICLE INFO

Keywords:

Si-jun-zi decoction
Renal fibrosis
Network pharmacology
Molecular docking
Experimental validation

ABSTRACT

Treating kidney diseases from the perspective of spleen is an important clinical method in traditional Chinese medicine (TCM) for anti-renal fibrosis (RF). Si-jun-zi decoction (SJZD), a classic formula for qi-invigorating and spleen-invigorating, has been reported to alleviate RF. This study aims to investigate the potential mechanism by which SJZD attenuates RF. The results demonstrated notable improvements in renal function levels, inflammation and fibrosis indices in UUO-mice following SJZD intervention. The main active ingredients identified were Quercetin, Kaempferol, Naringenin and 7-Methoxy-2-methyl isoflavone. Furthermore, STAT3, MAPK3, MYC were confirmed as key targets. Additionally, GO enrichment analysis demonstrated that SJZD delayed RF primarily by regulating oxidative stress and other biological mechanisms. KEGG enrichment analysis revealed the involvement of pathways such as Lipid and atherosclerosis signaling pathway, MAPK signaling pathway and other pathways in the reno-protective effects of SJZD. The molecular docking results revealed that the active ingredients of SJZD were well-bound and stable to the core targets. The experiments results revealed that Quercetin, Kaempferol, and Naringenin not only improved the morphology of TGF- β -induced HK-2 cells but also reversed the expression of α -SMA, COL1A1 and MAPK, thereby delaying the progression of RF. The anti-RF effects of SJZD were exerted through multi-components, multi-targets and multi-pathways.

1. Introduction

Renal fibrosis (RF) represents the final stage of most chronic or progressive kidney diseases, characterized by significant pathological changes including the extracellular matrix (ECM) synthesis, tubular epithelial morphological metamorphosis (EMT), oxidative stress and cytokine production. These changes ultimately lead to renal structural damage, loss of function and even end-stage renal disease (ESRD) [1,2]. For the majority of ESRD patients, renal replacement treatment becomes the primary strategy for prolonging

* Corresponding author. Department of Nephrology, Affiliated Huai'an Hospital of Xuzhou Medical University, Huai'an, Jiangsu, 223002, PR China.

** Corresponding author. Department of Nephrology, Affiliated Huai'an Hospital of Xuzhou Medical University, Huai'an, Jiangsu, 223002, PR China.

E-mail addresses: lihailun101@sina.com (H. Li), haeyzdh@163.com (D. Zheng).

¹ Sharing first authorship.

<https://doi.org/10.1016/j.heliyon.2024.e35489>

Received 12 April 2024; Received in revised form 21 July 2024; Accepted 30 July 2024

Available online 2 August 2024

2405-8440/© 2024 The Authors. Published by Elsevier Ltd. This is an open access article under the CC BY-NC license (<http://creativecommons.org/licenses/by-nc/4.0/>).

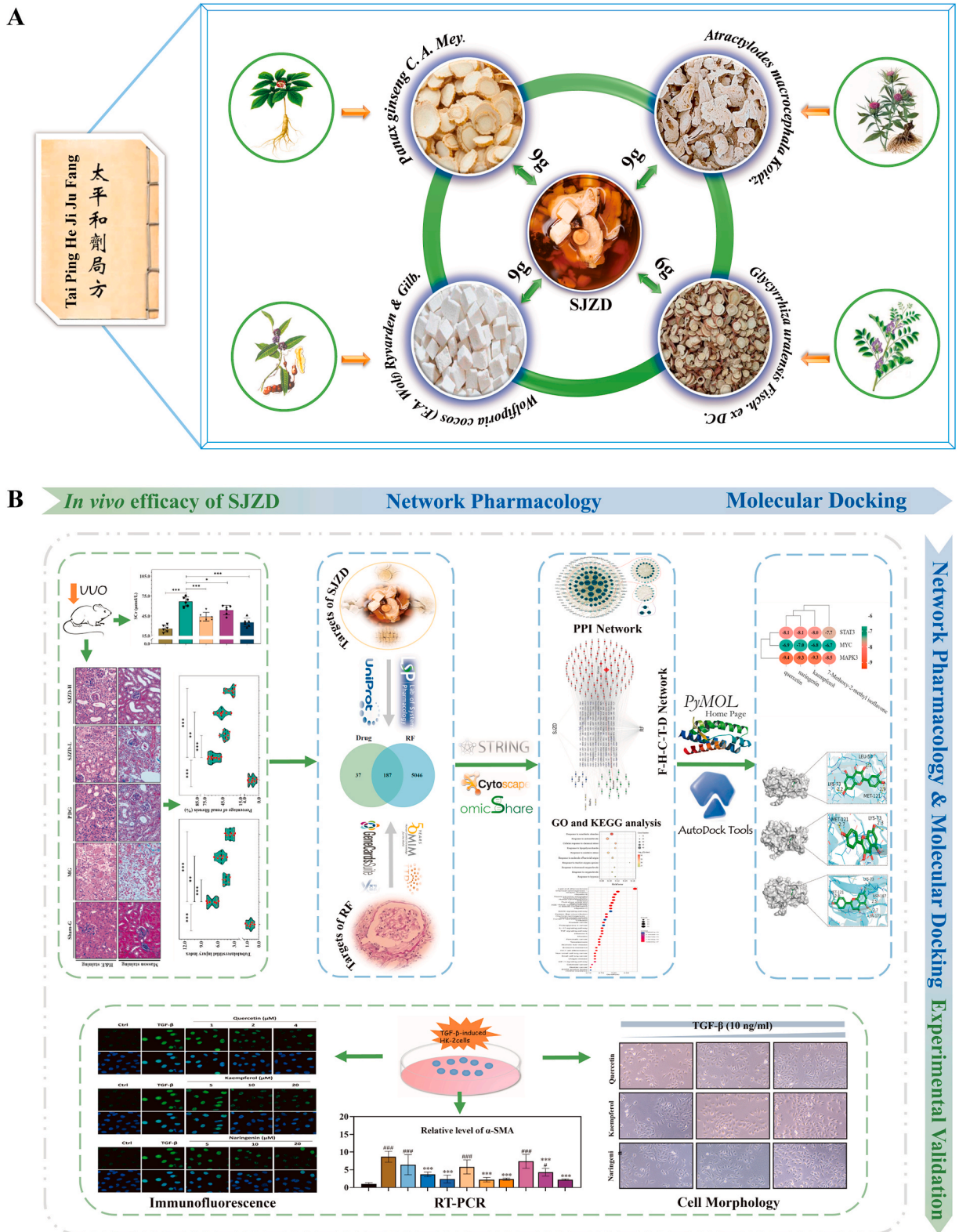


Fig. 1. (A) The composition and proportion of the herbs in SJZD. (B) The workflow of the entire research design.

survival. By 2040, it is estimated that 2.2 million individuals will succumb to CKD, with a worst-case scenario projecting up to 4 million [3]. It is therefore of the utmost importance to intervene at the earliest opportunity and to delay the progression of RF in the treatment of CKD.

Si-jun-zi decoction (SJZD), a well-known tonifying qi and invigorating spleen TCM formula, consists of *Panax ginseng* C. A. Mey. (Renshen), *Atractylodes macrocephala* Koidz. (Baizhu), *Wolfiporia cocos* (F.A. Wolf) Ryvarden & Gilb. (Fuling) and *Glycyrrhiza uralensis* Fisch. ex DC. (Gancao) with a proportion of 9:9:9:6 (Fig. 1A). The initial description of it date back to the Song Dynasty about 1000 years ago, in the classical medical text “Tai Ping He Ji Ju Fang” [4]. Mou Chonglin proposed that the activities of the human organs are based on the spleen and kidney, and the kidney is the continuation of the spleen [5]. Previous literature has also systematically discussed the theory of spleen and kidney, including its connotations, origins and clinical applications. This research has confirmed the interplay and influence between the spleen and kidney, leading to the development of common disease [6]. Furthermore, certain herbs of SJZD have been reported to possess anti-inflammatory and antioxidant properties [7–9]. Similarly, compounds or extracts from these herbs have demonstrated the ability to improve renal function, mitigate tubular oxidative damage, and impede the progression of RF [10–12]. Additionally, previous research has demonstrated that the incorporation of SJZD with Western medication significantly improves renal impairment in CKD patients at stages 3–5, thereby improving calcium and phosphorus metabolism and promoting overall body recovery [13]. Therefore, based on these theories and facts, we speculate that SJZD has some efficacy in the treatment of RF, but its target and mechanism have not been reported.

Network pharmacology has elucidated the intricate relationships between herbal formulas and diseases in a systematic manner, constructing a comprehensive network that encompass formulas, herbs, components, targets, and diseases (F–H–C–T–D network). This has enhanced our understanding of their interconnections [14]. It is highly advantageous in elucidating the intricate mechanisms of TCM treatment of diseases involving multiple components, targets, and pathways [15]. For example, Simiao Powder could prevent and treat Gout by improving metabolism and endocrine function, modulating immune and inflammatory responses [16]. Quercetin, Kaempferol and Wogonin, the main components of Huanglian Jiedu Tang, are believed to have therapeutic effects on sepsis [17]. Additionally, Danshen could increase the number of red blood cells by modulating the JAK-STAT signaling pathway, thereby alleviating anemia [18]. Molecular docking helps to predict the ligand-target binding modes and its affinities at the molecular level [19]. Binding energies lower than 0 kcal/mol indicate spontaneous binding of protein molecules to small molecules, below -5.0 kcal/mol suggest favorable binding activity and below -7.0 kcal/mol denote significant binding activity [20]. In this paper, the potential pharmacological mechanism of SJZD anti-RF was explored in depth with the help of network pharmacology and molecular docking, and the results obtained were validated by *in vitro* cellular experiments. Fig. 1B illustrates the workflow of the entire research design.

2. Materials and methods

2.1. Reagents

The purchase of Fosinopril was from Bristol-Myers Squibb Co., Ltd. (New York, USA). Masson trichrome and hematoxylin and eosin (H&E) staining kits were bought from Leagene Biotechnology Co., Ltd. (Beijing, China). Detection kits, including serum creatinine (SCr) and blood urea nitrogen (BUN), were bought from Jiancheng Biotechnology Co., Ltd. (Nanjing, China). HK-2 cells were bought from MeisenCTCC (Zhejiang Meisen Cell Technology Co., Ltd). DMEM high sugar culture medium and premium fetal bovine serum (FBS) were bought from Wuhan Punosai Life Technology Co., Ltd. CCK8 reagent kit purchased from Shanghai White Shark Biotechnology Co., Ltd. Quercetin (HY-18085), Kaempferol (HY-14590) and Naringenin (HY-W011641) were acquired from MedChemexpress (MCE) Biotechnology Co., LTD. AG RNAex Pro RNA kit (AG21102), Evo M-MLV reverse transcription Kit (AG11728) and SYBR® Green Pro Taq HS premixed type qPCR kit (AG11701) were bought from Accurate Biology (Hunan Accurate Biology Technology Co., Ltd). Primary and secondary antibodies utilized in this study were procured from Abcam Co., Ltd. (Cambridge, United Kingdom).

2.2. Animals

Male BALB/c mice (7 ± 1 weeks old, 20 ± 2 g) were procured from the Animal Center of Xuzhou Medical University. They were kept in an animal laboratory under standardized conditions (22 ± 2 °C, 65 ± 5 % relative humidity, 12 h light-dark cycle). Each animal had sufficient distilled water and standard food. The research was conducted in accordance with the protocols specified in the Guide for the Care and Use of Laboratory Animals. The Ethics Committee of Xuzhou Medical University supervised the animal studies and treatment protocols (Ethics Approval Number: L20210226229).

2.3. Establishment of UUO-model and further drug administration regimens

The RF model was generated using the left renal unilateral ureteral obstruction (UUO) operation surgical technique, following the established procedure as previously described in the literature [21]. According to our previous study [22], the dosages of SJZD-L and SJZD-H were set to 200 mg/kg/d and 800 mg/kg/d, respectively. Meanwhile, the dosage of fosinopril (positive drug) was set at 10 mg/kg according to a previous report [21].

A randomized method was used to assign the mice into 5 groups ($n = 8$), including Sham-operation control group (Sham-G, saline), model group (MG, UUO + saline), positive drug group (PDG, UUO + fosinopril), low-dose group of SJZD (SJZD-L, UUO + SJZD) and high-dose group of SJZD (SJZD-H, UUO + SJZD) for a 7-day drug intervention. Then, mice were anesthetized by intraperitoneal

injection of 10 % pentobarbital sodium (3 ml/kg). Following the collection of blood samples, they were immediately executed by cervical dislocation, and the renal tissue was promptly isolated for subsequent experiments.

2.4. Renal function examination

The levels of BUN and SCr were determined by employing appropriate detection kits, following the manufacturer's instructions.

2.5. Renal histopathological examination

Renal tissue slices were stained with hematoxylin and eosin (H&E) or Masson's trichrome, following the manufacturer's protocols. Histological data was obtained by 2 independent observers in a blinded manner. The degree of inflammation was assessed and scored according to established methodology [23]. The extent of RF was observed according to the area of fibrosis staining.

2.6. Bioactive components and related targets of SJZD

Bioactive ingredients of SJZD were retrieved from Traditional Chinese Medicines Systems Pharmacology Platform (TCMSP, <https://tcmspw.com/tcmsp.php/>) [24]. The active components were evaluated by considering their ADME properties including absorption, distribution, metabolism and excretion. Specifically, we focused on selecting with drug-like properties (DL) of at least 0.18 and ensuring an oral-bioavailability (OB) of at least 30 %. Meanwhile, targets linked to these bioactive components were identified from TCMSP and normalized in the Uniprot database (<https://www.uniprot.org/>).

2.7. Potential targets of RF

Using "renal fibrosis" as the search term, targets associated with RF were retrieved from 4 databases, namely TTD (Therapeutic Target Database, <https://db.idrblab.net/ttd/>), OMIM (Online Mendelia Inheritance in Man, <https://omim.org/>) and PharmGkb (<https://www.pharmgkb.org/>), GeneCards (<https://www.genecards.org/>). Venn diagrams were plotted using R software to show the intersection of targets related to RF and SJZD.

2.8. F-H-C-T-D and C-T networks

Cytoscape 3.7.0, the visualization tool, was employed to construct F-H-C-T-D and C-T networks. In these networks, "nodes" represent formulas, herbs, active components, gene targets, and diseases, while "edges" represent the relationship between nodes. Additionally, the node degree values were used to confirm the main active components within the C-T network. The greater the degree value of a node, the higher its significance [25]. In this study, nodes with the degree values greater than two times the average degree value were considered as the main components.

2.9. PPI network

After submitting 187 overlapping targets of SJZD and RF active components to String online database (<https://string-db.org/>), the PPI network was constructed using the following settings: selecting "Multiple proteins" option, specifying "*Homo sapiens*", setting the confidence level " ≥ 0.9 ", and hiding discontinuous nodes within network. The PPI network database was then exported and loaded into Cytoscape for further research, including calculation of topological parameters and identification of core targets. The topological parameters, namely Betweenness centrality (BC), Closeness centrality (CC), Degree centrality (DC), Eigenvector centrality (EC), Local average connectivity (LAC) and Network centrality (NC), were calculated in Cytoscape using the CytoNCA plug-in [26]. Nodes with values above the median of topological parameters were selected to construct a sub-network for further analysis. Similarly, the preservation condition in the new sub-network remains unchanged, and the core targets of PPI network was ultimately generated after 3 filters.

2.10. GO and KEGG analysis

R software and its related packages, including "clusterProfiler", "org.Hs.eg.db", "enrichplot", "ggplot2" and "pathview packages" were applied to perform gene target enrichment analysis. To filter the results, both *P*-value and corrected *P*-value (*q*-value) were employed, with a threshold of ≤ 0.05 . The top 10 GO-terms of each GO and top 30 KEGG pathways were selected for the chart. Subsequently, a total of 30 signaling pathways and their corresponding intersection targets were imported into Cytoscape to establish P-T network and computed the degree values of nodes within network.

2.11. Molecular docking

The 2D structures of SJZD's active component were retrieved from the PubChem database (<https://pubchem.ncbi.nlm.nih.gov/>) and then converted to 3D structures, The 3D structures were optimized for minimum free energy and saved as a small molecule ligand in "Mol2" format using Chem3D software. The 3D structure PDB format documents of the core targets were found from the RCSB-PDB

database (<https://www.rcsb.org/>). PyMol 2.4.1 was utilized to remove water and heterogeneous molecules from protein receptor files, which were saved in “pdb” format. Furthermore, both ligand and receptor underwent processing using Autodock tools 1.5.6, with the ligands converted to “PDBQT” format. The receptor’s secondary structure was displayed and the grid box parameters were adjusted to ensure complete concealment of the receptor. Then, molecular docking was performed using Vina to calculate binding energy three times. Finally, the docking model with the lowest binding energy was visualized using Pymol 2.4.1, a visualization tool, to investigate detailed information about the interaction between the main active ingredients and targets.

2.12. Cell viability

To evaluate the viability of TGF- β , Quercetin, Kaempferol, and Naringenin on HK-2 cells, 4×10^3 cells/well were cultured in 96-well plates until completely adherent. Following incubation with Quercetin (1, 2, 4, 8, 16, 32, 64 or 128 μ M), or Kaempferol/Naringenin (1, 5, 10, 20, 40, 80, 160 or 320 μ M) for 48h, cells were subjected to further treatment with or without TGF- β (10 ng/ml) for another 48 h. In addition, control well (excluding TGF- β , Quercetin, Kaempferol and Naringenin) and model well (10 ng/ml TGF- β) were set up, and CCK-8 reagent was added to each well. After 4 h of incubation, the Microplate Reader was utilized to record absorbance (A) at 450 nm.

2.13. Culture, model construction, and administration of HK-2 cells

The cells were incubated in dulbecco’s modified eagle medium (DMEM) high-sugar medium, which was supplemented with 10 % fetal bovine serum (FBS) and 1 % penicillin-streptomycin. To induce fibrosis, the cells were cultured in TGF- β at a concentration of 10 ng/ml for 48 h. The experimental groups included a control group (equal amount of solvent), model group (10 ng/ml TGF- β), low-dose Quercetin/Kaempferol/Naringenin group (10 ng/ml TGF- β + 1 μ M Quercetin/5 μ M Kaempferol or Naringenin), middle-dose Quercetin/Kaempferol/Naringenin group (10 ng/ml TGF- β + 2 μ M Quercetin/10 μ M Kaempferol or Naringenin), high-dose Quercetin/Kaempferol/Naringenin group (10 ng/ml TGF- β + 4 μ M Quercetin/20 μ M Kaempferol or Naringenin).

2.14. Cell morphology

HK-2 cells were cultured in 6-well plates at a density of 2×10^5 cells/ml at 37 °C and 5 % CO₂. The control group was added to the FBS-containing culture medium directly, while the corresponding drug-containing serum culture medium was added according to groups. Subsequently, TGF- β was stimulated at a concentration of 10 ng/ml for 48 h in accordance with the protocol of each corresponding group, and the morphological alterations of the cells within each group were examined using an inverted microscope.

2.15. RT-PCR

HK-2 cells were seeded at a density of 1×10^5 cells/ml in 12-well plates and subjected to the appropriate interventions. Following this, they were washed 3 times with phosphate-buffered saline (PBS). RNA extraction was performed using the AG RNAex Pro kit following the instructions provided. The quality and concentration of the extracted RNA were assessed using a Nanodrop spectrophotometer. RNA was extracted and reverse transcribed into cDNA using the Evo M-MLV reverse transcription kit. The resulting cDNA was then subjected to Premixed SYBR® Green Pro Taq HS qPCR amplification reactions using a PCR kit. The amplification protocol consisted of an initial pre-denaturation phase at 95 °C for 30s, followed by 40 cycles. Each cycle involved a denaturation process at 95 °C for 5 and annealing at 60 °C for 30s. The mRNA expression levels were assessed using the commonly used $2^{-\Delta\Delta Ct}$ technique, with the β -actin gene serving as an internal reference. The forward primer for COL1A1 is 5'-GGGTCTAGACATGTTTCAGCTTTGTG-3', and the reverse primer is 5'-ACCCCTAGGCCATTGTGTATGC-3'. Meanwhile, the forward primer for α -SMA is 5'-GTCCCAGACATCAGGGAGTAA-3', and its reverse primer is 5'-TCGGATACTTCAGCGTCAGGA-3'.

2.16. Immunofluorescence

Immunofluorescence was used to evaluate the expression levels of MAPK, α -SMA and COL1A1 in HK-2 cells. The cells were seeded onto pre-coated cell slides in a 24-well plate at a density of 1×10^4 cells/ml during their logarithmic proliferation phase. Following the removal of the culture medium, the cells were washed 3 washes with PBS and then fixed with 4 % paraformaldehyde for 15 min. After fixation, they were permeabilized with 0.5 % Triton X-100 for 15 min and then sealed with goat serum for 30 min prior to an overnight incubation at 4 °C with primary antibodies. Following 3 washes with PBS, the cells were treated with fluorescent secondary antibodies at 37 °C for 60 min. Following another round of washing, DAPI was added to the cells for 5 min before fluorescence images were captured using fluorescence microscopy. The fluorescence density values were calculated using Image J software to analyze the obtained images.

2.17. Correlation analysis

Following the standardization of the model group, fibrosis index and protein data were standardized for each group. Intra-group correlation analysis was performed between protein expression and fibrosis index parameters in each group.

2.18. Statistical analysis

Graphpad Prism 9.5.1 was conducted for statistical analysis. All experimental data were reported as means \pm standard deviation (SD). One-way ANOVA was employed to analyze the statistical significance of mean differences, which were subsequently subjected to Tukey's multiple comparison test. The significance level was set at $P < 0.05$.

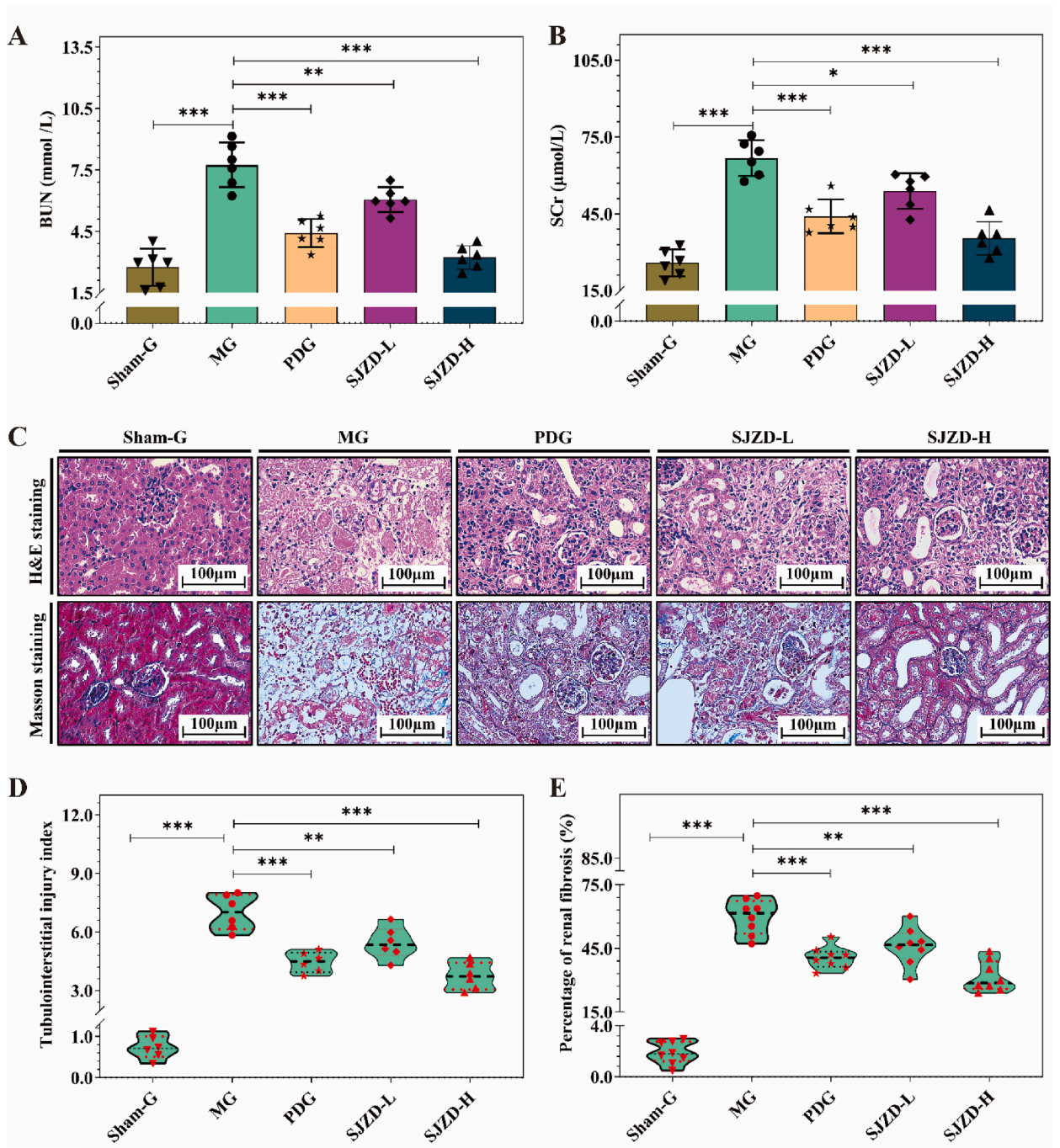


Fig. 2. The levels of BUN (A) and SCr (B) in UUO-mice. (C) Representative micrographs of renal tissues with H&E and Masson trichrome staining. (D) The renal tubulointerstitial injury index was scored according to H&E staining. (E) Percentage of positive Masson staining in the renal tubulointerstitial region relative to the entire region. Data are represented as mean \pm SD. Superscript letters *, ** and *** denoted $P < 0.05$, $P < 0.01$ and $P < 0.001$, respectively.

3. Results

3.1. SJZD efficacy in UUO-mice

As RF progressed, there was a gradual decline in renal function. therefore, the therapeutic efficacy of SJZD was evaluated by measuring the indicators of renal function (BUN, SCr), as well as tubulointerstitial injury index and the degree of RF. The results depicted in Fig. 2A–E demonstrate significant improvements in BUN, SCr levels, tubulointerstitial damage index (based on H&E staining) [23], and RF percentage (based on Masson staining) in MG compared to the Sham-G ($P < 0.001$). This indicated that the UUO-mice model was successfully established. The PDG, SJZD-L, and SJZD-H groups showed significant reductions in these parameters in comparison with the MG ($P < 0.05$, $P < 0.01$, and $P < 0.001$, respectively). Additionally, the administration of SJZD resulted in a dose-dependent down-regulation of the above 4 indicators. The findings of this investigation indicate that the administration of SJZD may have a potentially beneficial effect in mitigating the decline in renal function and fibrosis caused by UUO surgery.

3.2. SJZD anti-RF potential targets

After satisfying the screening standard, 136 bioactive components of 4 herbal medicines in SJZD were finally obtained by searching the TCMSP. Specifically, there were 22 components were found in Renshen, 15 in Fuling, 7 in Baizhu and 92 in Gancuo (Table S1). Meanwhile, 224 targets related to these herbals (Table S2) were identified. Furthermore, 5,233 RF-related targets were found using GeneCards, TTD, OMIM, and PharmGkb disease gene databases (Fig. 3A, Table S3). Based on these retrieved targets of bioactive components and RF, a total of 187 intersection targets were eventually identified by Venn diagram drawn by R software, as shown in Fig. 3B (Table S4). These results suggested that SJZD may treat RF through 187 different target genes.

3.3. F–H–C–T–D and C–T networks

The F–H–C–T–D network consisted of 304 nodes and 1,749 edges, including 111 bioactive component nodes, 187 intersection gene target nodes, 4 herbal nodes, 1 formula node and 1 disease node (Fig. 4A). As shown in Fig. 4A, the active components of 4 herbs in SJZD affected the development of RF by acting on one or more target genes. These data are consistent with the attributes of multi-component and multi-target approach to anti-RF in TCM. The compounds and intersection target data in Fig. 4A were stripped to further construct the C–T network (Fig. 4B) to ascertain the main active components. In addition, the degree value of active components within the C–T network was calculated using topological analysis (Table S5). Ingredients with degree values more than twice the mean value were identified as the main active ingredients, namely Quercetin, Kaempferol, Naringenin and 7-Methoxy-2-methyl isoflavone, respectively. Table 1 provides the detailed information of the 4 active ingredients.

3.4. PPI network

The PPI network (Fig. 5A a) with 159 nodes and 1,512 edges was queried using String database after the specified conditions were met. Nodes in the network symbolize protein names, while edges stand for proteins interactions. To determine the core targets of SJZD anti-RF, we loaded its data into Cytoscape to establish a new network (Fig. 5A b). Subsequently, we employed the CytoNCA plug-in within the Cytoscape to compute topological parameters [27] and detect core targets. The selection threshold was determined based on the corresponding median values. Specifically, BC, CC, DC, EC, LAC and NC exceeded 57.336, 0.103, 14, 0.041, 5.091, and 5.818 respectively (Results are retained to 3 decimal places). Gene targets meeting the conditions were selected and colored blackish-green in Fig. 5A b, forming a sub-network with 45 nodes and 608 edges (Fig. 5A c). Similarly, gene targets that met the conditions (BC, CC, DC, EC, LAC, NC exceeded 17.202, 0.571, 24, 0.127, 12, and 13.169, respectively) were selected and colored blackish-green in Fig. 5A c, and the new sub-network comprising of 17 nodes and 194 edges was constructed (Fig. 5A d). Finally, gene targets that met the standard (BC, CC, DC, EC, LAC, NC exceeded 4.443, 0.8, 24, 0.249, 16.334, and 18.862, respectively) were picked and colored blackish-green (Fig. 5A d), which was used to build sub-network comprising of 3 nodes and 6 edges (Fig. 5A e). Therefore, STAT3, MAPK3, MYC might be significantly involved in the treatment of SJZD in RF. Meanwhile, Fig. 5B displayed the topological parameter values of the core

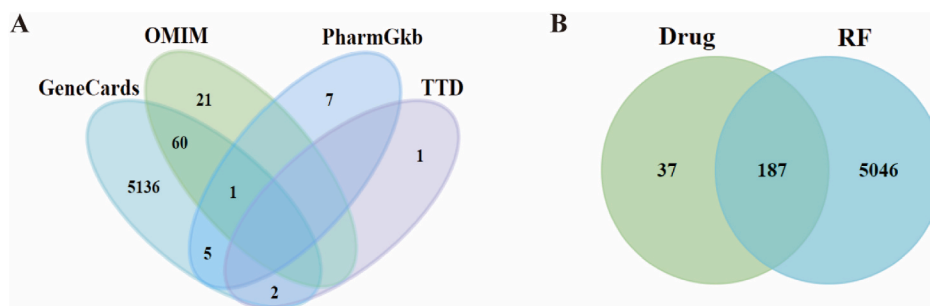


Fig. 3. (A) RF-related potential targets from 4 databases. (B) The intersection gene targets of RF and SJZD.

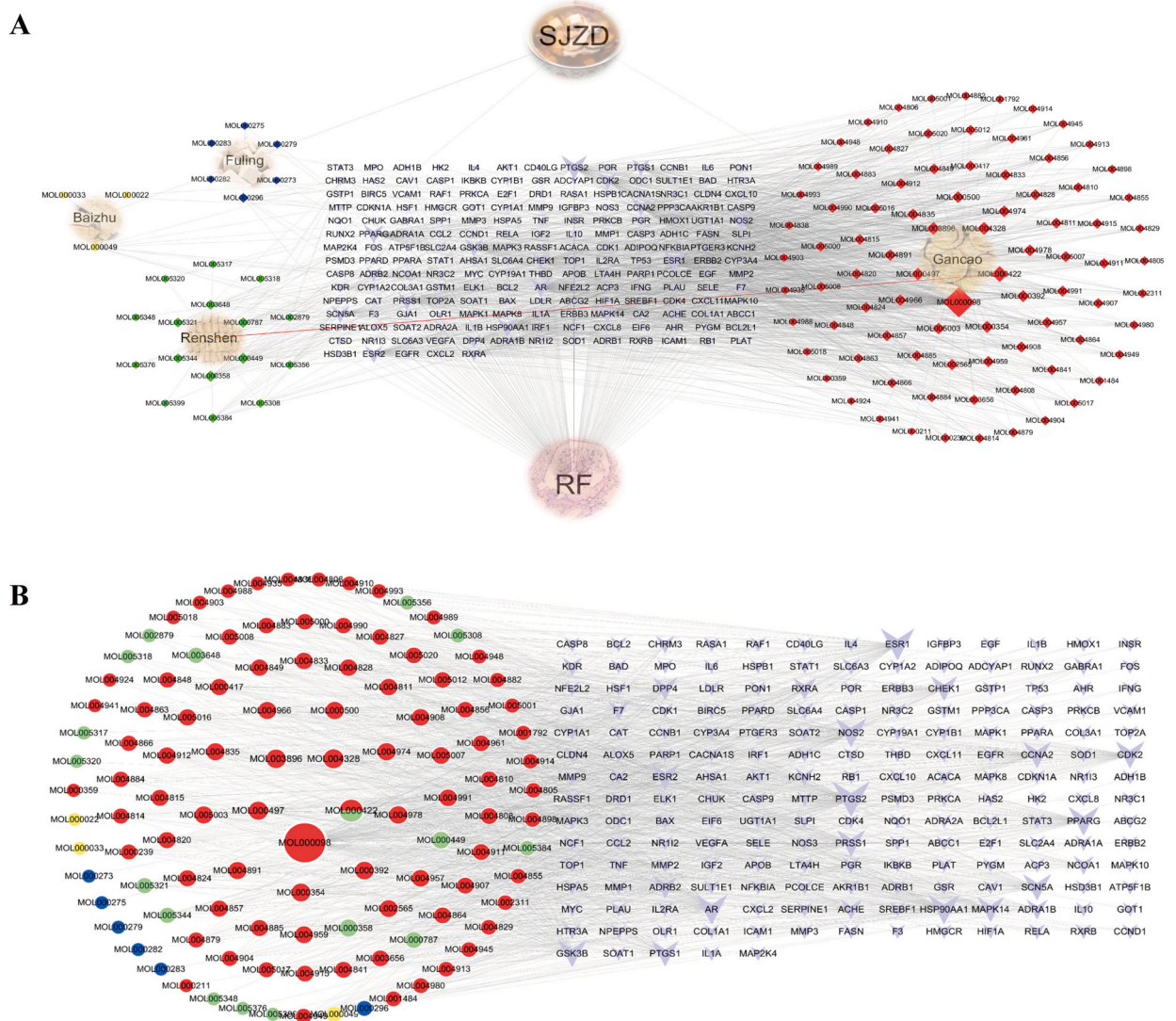


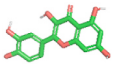
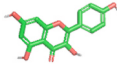
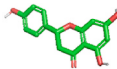
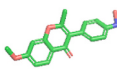
Fig. 4. (A) F-H-C-T-D network. The representatives of V nodes indicate gene targets of RF. The diamond nodes stand for active components. The red line indicated that Kaempferol came from both Gancao and Renshen. (B) C-T network. The representatives of V nodes indicate gene targets of RF. Different colors of the pie chart display that the components are from different Chinese herbs, red figures Gancao, green shows Renshen, blue represents Fuling and yellow demonstrates Baizhu. (For interpretation of the references to color in this figure legend, the reader is referred to the Web version of this article.)

target. The results of the 3 times topological parameters were listed in the supplementary materials (Table S6).

3.5. GO and KEGG analyses

The analysis yielded 2,839 significant GO-terms, including 2,531 BP GO-terms, 86 CC GO-terms, and 222 MF GO-terms ($P < 0.05$) (Table S7). In BP, we identified multiple GO-terms linked to mitochondria, which were subsequently grouped into mitochondrial function. Then the top 10 GO-terms are shown in Fig. 6A. This indicated that the potential targets for SJZD in RF therapy were primarily centered on BP, such as Response to oxidative stress (GO:0006979), Response to lipopolysaccharide (GO:0032496) and Mitochondrial function (Examples include Apoptotic mitochondrial changes, Regulation of mitochondrial organization, etc.), whereas CC analysis mainly involved in Membrane raft (GO:0045121), Membrane microdomain (GO:0098857), Vesicle lumen (GO:0031983), etc. and MF analysis mainly enriched in DNA-binding transcription factor binding (GO:0140297), Receptor ligand activity (GO:0048018), among others. Details of the targets involved in the top 10 ranked mitochondrial functions are shown in Fig. 6B. In addition, the core targets involved in the top 10 highly enriched GO terms of BP, CC and MF were demonstrated in Fig. 6C. We discovered that the core target MAPK3 was mainly involved in 6 GO-terms of BP, 4 GO-terms of CC and 1 GO-terms of MF, while MYC mainly involved in 2 GO-terms of BP and 3 GO-terms of MF, and STAT3 involved in 4 GO-terms of MF and 1 GO-terms of BP.

Table 1
Main active components.

| Components | MF | Molecular weight | 2D Structure diagram | OB (%) | DL | Degree |
|-------------------------------|--|------------------|---|--------|------|--------|
| Quercetin | C ₁₅ H ₁₀ O ₇ | 302.25 |  | 46.43 | 0.28 | 127 |
| Kaempferol | C ₁₅ H ₁₀ O ₆ | 286.25 |  | 41.88 | 0.24 | 45 |
| Naringenin | C ₁₅ H ₁₂ O ₅ | 272.27 |  | 59.29 | 0.21 | 30 |
| 7-Methoxy-2-methyl isoflavone | C ₁₇ H ₁₃ O ₅ | 266.31 |  | 42.56 | 0.2 | 28 |

In KEGG analysis, a total of 176 RF genes were mapped into the KEGG database as the background gene set (Table S8). Significant association was then observed with 180 pathways identified using a threshold of $P < 0.05$. The top 30 pathways were selected for visualizations as depicted in Fig. 7A. Cytoscape was utilized to analyze the gene targets and pathway data (Fig. 7B) to further elaborate the association between targets and the top 30 pathways and to identify crucial pathways involved in SJZD anti-RF. MAPK3 was associated with 26 pathways including Lipid and atherosclerosis (hsa05417), AGE-RAGE signaling pathway in diabetic complications (hsa04933), Fluid shear stress and atherosclerosis (hsa05418), etc. AGE-RAGE signaling pathway in diabetic complications (hsa04933) was related to 33 gene targets such as MAPK3, STAT3, RELA, MAPK1, etc. These findings confirm the multi-target and multi-channel properties of SJZD. The CytoNCA plug-in within Cytoscape was then employed to calculate the topology parameters of pathways and to explore major pathways. Only pathways with DC value higher than the median (29.97) were considered as main pathways (Table S9). As a result, pathways such as Lipid and atherosclerosis (hsa05417), AGE-RAGE signaling pathway in diabetic complications (hsa04933), Fluid shear stress and atherosclerosis (hsa05418), Chemical carcinogenesis-reactive oxygen species (hsa05208), MAPK signaling pathway (hsa04010), etc. play a huge part in the treatment of RF in SJZD.

3.6. Molecular docking results

Table 1 provides an overview of the main bioactive components of SJZD that are believed to be responsible for its therapeutic effects in the treatment of RF. The identified bioactive components include Quercetin, Kaempferol, Naringenin and 7-Methoxy-2-methyl isoflavone. Based on Fig. 5A, we identified MYC, STAT3 and MAPK3 as core targets. The average docking results of main components with core targets were shown in Fig. 8A (Results are maintained to one decimal place. Detailed scoring data are listed in Supplementary Material Table S10). Among them, MAPK3 had the lowest binding energy to Quercetin (-9.4 kcal/mol), whereas MYC had the highest binding energy to 7-Methoxy-2-methyl isoflavone (-6.7 kcal/mol). Thus, four specific compounds (Quercetin, Kaempferol, Naringenin, and 7-Methoxy-2-methyl isoflavone) found in SJZD were shown to bind well to 3 core targets of RF (MAPK3, MYC, STAT3). These targets are believed to be significantly involved in the intervention of RF.

Besides, the main bioactive components and key targets with average docking binding energy < -9 kcal/mol were selected for further analysis (Table 2). According to Table 2, the specific combined sites of ligands and receptors were visualized in Fig. 8B. Such as MAPK3 (7NRB) and Quercetin bind to ASP-187, LYS-73, and MET-121 residues via 4 hydrogen bonds with hydrogen bond lengths of 2.9, 3.2, 3.4 and 2.4, respectively. MAPK3 (7NRB) and Kaempferol bind to MET-121, LYS-73 and LEU-50 residues through 3 hydrogen bonds with hydrogen bond lengths of 3.2, 3.3 and 2.0, respectively. MAPK3 (7NRB) and Naringenin bind to MET-121 and LYS-73 residues via 2 hydrogen bonds with hydrogen bond lengths of 3.3 and 3.3, respectively.

3.7. Results of cell viability

From Fig. 9A–C, we can see that Quercetin (at concentrations of 1–32 μ M), Kaempferol (at concentrations of 1–20 μ M) and Naringenin (at concentrations of 1–40 μ M) exhibited minimal effect on cell activity in comparison to the control group. From Fig. 9D–F, we also found that under 10 ng/ml TGF- β coordinated intervention, the appropriate concentrations of Quercetin, Kaempferol and Naringenin also demonstrated minimal effects on cell activity when compared to the control group. Therefore, for subsequent research, the administration concentrations were selected as follows: Quercetin (at concentrations of 1, 2 and 4 μ M), Kaempferol (at concentrations of 5, 10 and 20 μ M) and Naringenin (at concentrations of 5, 10 and 20 μ M).

3.8. Cell morphology and α -SMA, COL1A1 expression

As illustrated in Fig. 10A, cells in control group were in good condition, exhibiting cobblestone-like changes and tight intercellular spaces. In contrast, after 48 h of stimulation with TGF- β , cells in model group had extended cytoplasm and expanded intercellular

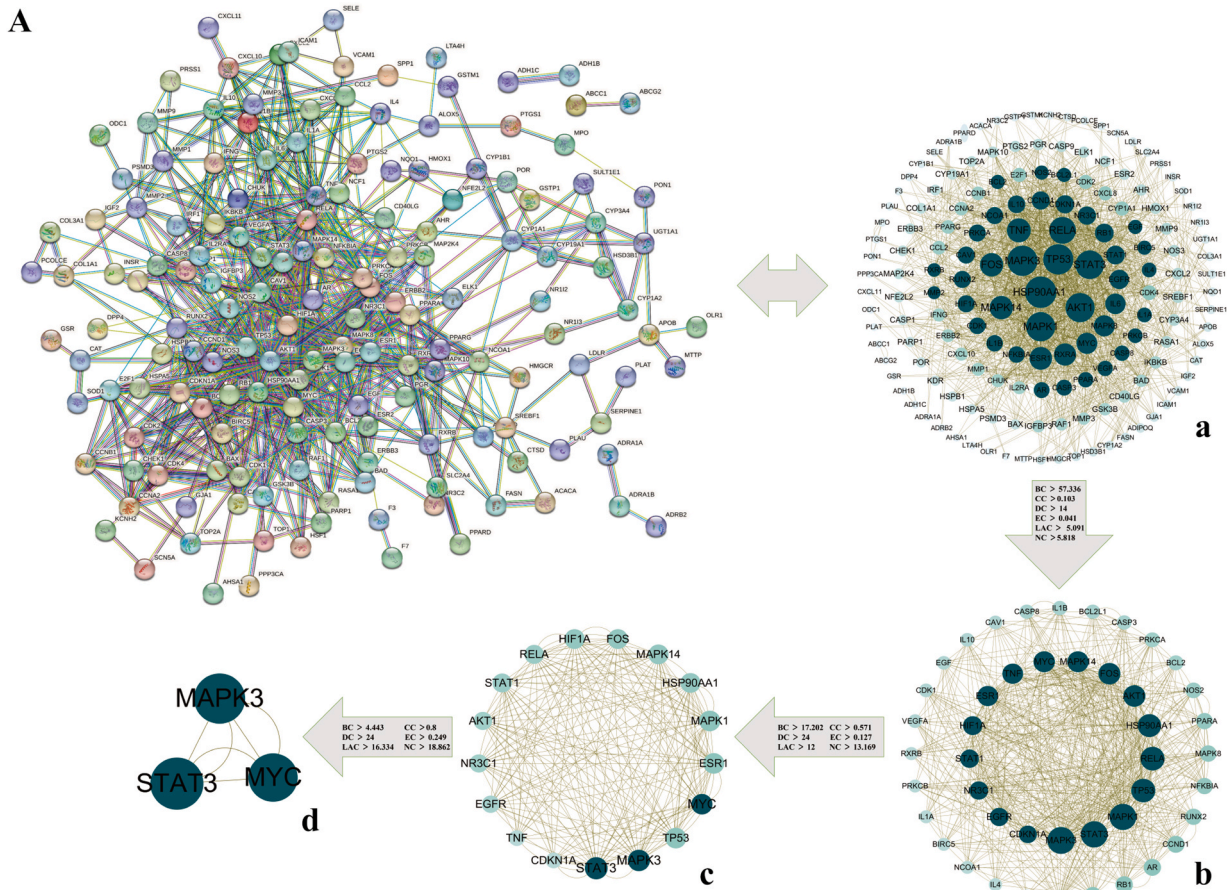


Fig. 5. (A) PPI network. (a) PPI network. It comprises 159 nodes and 1,512 edges. Each node represents relevant targets, and edges stand for protein-protein associations. (b) PPI network imported from String database to Cytoscape 3.7.0. (c) Sub-network of significant targets extracted from (b) by filtering 6 parameters: BC, CC, DC, EC, NC and LAC. This network is made up of 45 nodes and 608 edges. (d) Sub-network of more significant targets extracted from (c) by filtering 6 parameters: BC, CC, DC, EC, NC and LAC. This network is made up of 17 nodes and 194 edges. (e) Sub-network of core targets extracted from (d) by filtering 6 parameters: BC, CC, DC, EC, NC and LAC. This network is made up of 3 nodes and 6 edges. (B) Topology parameter values of core targets.

spaces, resembling the form of elongated shuttles. Following intervention with different concentrations of Quercetin, Kaempferol and Naringenin, the majority of cells were able to reverse the stimulation of TGF- β on the morphological changes of HK-2 cells, and reduction of shuttles could be seen in the cell morphology, the cells became oval-shaped with tighter gaps, and morphological

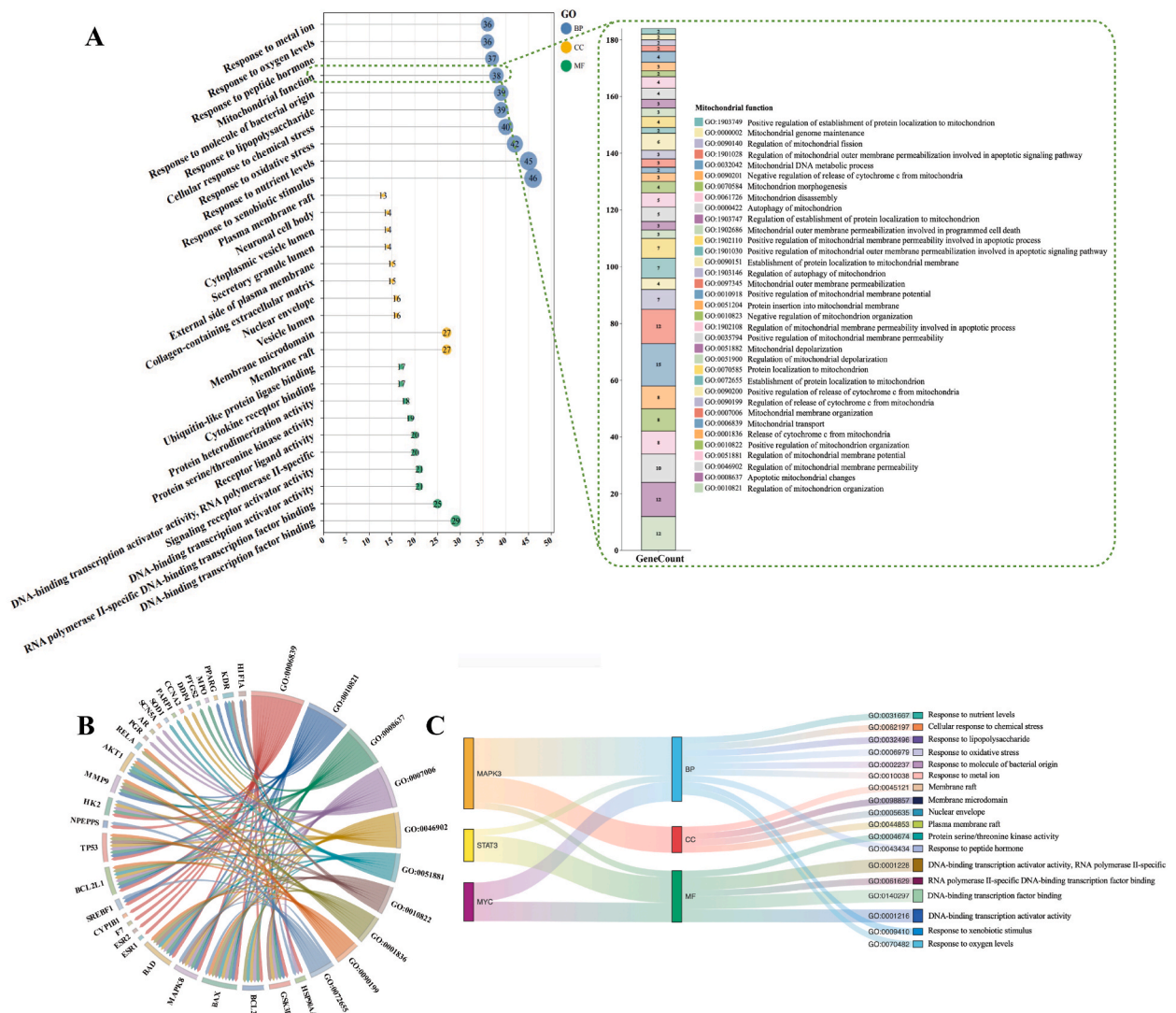



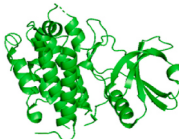
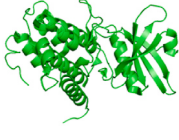
Fig. 6. (A) The top 10 GO-terms of BP/CC/MF for SJZD anti-RF and GO-terms of mitochondrial function. (B) Targets involved in the top 10 mitochondrial function. (C) Core targets among the top 10 significantly enriched GO terms in BP, CC and MF.

alterations closely resembled those observed in the control group, particularly in the high-dose group. Immunofluorescence observations revealed that the model group exhibited more pronounced strong fluorescence signals for α -SMA and COL1A1 proteins in comparison to the control group. Whereas the fluorescence signal intensity decreased in a dose-dependent manner after the intervention of different concentrations of Quercetin, Kaempferol and Naringenin (Fig. 10A and B). Similarly, RT-PCR experiment showed that Quercetin, Kaempferol and Naringenin dose-dependently reversed the TGF- β -induced expression of α -SMA and COL1A1 (Fig. 10C). Collectively, these findings suggest that 10 ng/ml TGF- β could induce fibrosis in HK-2 cells, but treatment with Quercetin, Kaempferol and Naringenin could abrogate TGF- β -induced fibrosis formation.

3.9. MAPK expression

According to Fig. 11A–B, it was observed that the MAPK protein in the model group exhibited a strong fluorescence signal compared to the control group. Upon treatment with varying concentrations of Quercetin, Kaempferol and Naringenin, the levels of fluorescence signal emitted by MAPK protein exhibited a reduction that was proportional to the dosage. Notably, the fluorescence signal intensity of high-dose group was nearly indistinguishable from that of the control group. The findings suggest that Quercetin, Kaempferol, and Naringenin have the potential for suppressing MAPK expression in HK-2 cells induced by TGF- β .

Table 2
Molecular docking test with average binding energy greater than 9 (kcal/mol).

| Target | PDB ID | 3D structure | Main components | Binding Energy (kcal/mol) | Grid Box | | Amino Acid Residue | H-bond length (Å) | | |
|------------|--------|---|-----------------|---------------------------|-----------|---------|--------------------|-------------------|---------|-----|
| | | | | | Center | Size | | | | |
| MAPK3 | 3FXW |  | Quercetin | -9.6 | X = | X = | LEU-50 | 2.1 | | |
| | | | | | 20.521 | 36 | | | LYS-73 | 2.2 |
| | | | | | Y = | Y = | | | | |
| | | | -5.431 | 48 | | | | | | |
| | | | Z = 13.042 | Z = | MET-121 | 2.9 | | | | |
| | | | | 48 | | | | | | |
| | | | | 48 | | | | | | |
| | | | Kaempferol | -9.5 | X = | X = | MET-121 | 2.7 | | |
| | | | | | 20.521 | 36 | LYS-73 | | 2.3 | |
| Y = | Y = | | | | | | | | | |
| -5.431 | 48 | | | | | | | | | |
| Z = 13.042 | Z = | | | | | | | | | |
| | 48 | | | | | | | | | |
| | 48 | | | | | | | | | |
| Naringenin | -9.4 | X = | X = | MET-121 | 2.8 | | | | | |
| | | 20.521 | 36 | ASN-171 | | 2.7 | | | | |
| | | Y = | Y = | | | | | | | |
| -5.431 | 48 | | | | | | | | | |
| Z = 13.042 | Z = | ASP-187 | 2.5 | | | | | | | |
| | 48 | | | | | | | | | |
| | 48 | | | | | | | | | |
| 7NRB | |  | Quercetin | -9.7 | X = | X = | LYS-73 | 2.2 | | |
| | | | | | 21.077 | 32 | | | ASP-187 | 2.9 |
| | | | | | Y = | Y = | | | | |
| | | | -5.468 | 48 | | | | | | |
| | | | Z = 12.953 | Z = | MET-121 | 3.4/2.4 | | | | |
| | | | | 48 | | | | | | |
| | | | | 48 | | | | | | |
| | | | Kaempferol | -9.8 | X = | X = | MET-121 | 3.2 | | |
| | | | | | 21.077 | 32 | LYS-73 | | 3.3 | |
| Y = | Y = | | | | | | | | | |
| -5.468 | 48 | | | | | | | | | |
| Z = 12.953 | Z = | LEU-50 | 2.0 | | | | | | | |
| | 48 | | | | | | | | | |
| | 48 | | | | | | | | | |
| Naringenin | -9.7 | X = | X = | MET-121 | 3.3 | | | | | |
| | | 21.077 | 32 | LYS-73 | | 3.3 | | | | |
| | | Y = | Y = | | | | | | | |
| -5.468 | 48 | | | | | | | | | |
| Z = 12.953 | Z = | | | | | | | | | |
| | 48 | | | | | | | | | |
| | 48 | | | | | | | | | |
| 3R1N | |  | Quercetin | -8.9 | X = 12.08 | X = | ASP-187 | 2.5 | | |
| | | | | | | 32 | | | ASN-171 | 2.7 |
| | | | | | Y = 0.652 | Y = | | | | |
| | | | | 46 | | | | | | |
| | | | Z = 15.973 | Z = | MET-121 | 2.9 | | | | |
| | | | | 48 | | | | | | |
| | | | | 48 | | | | | | |
| | | | Kaempferol | -8.6 | X = 12.08 | X = | MET-121 | 2.8 | | |
| | | | | | | 32 | THR-186 | | 2.4 | |
| Y = 0.652 | Y = | | | | | | | | | |
| | 46 | | | | | | | | | |
| Z = 15.973 | Z = | ASN-171 | 2.6 | | | | | | | |
| | 48 | | | | | | | | | |
| | 48 | | | | | | | | | |
| Naringenin | -8.8 | X = 12.08 | X = | ASP-187 | 2.1 | | | | | |
| | | | 32 | ASN-171 | | 2.6 | | | | |
| | | Y = 0.652 | Y = | | | | | | | |
| | 46 | | | | | | | | | |
| Z = 15.973 | Z = | | | | | | | | | |
| | 48 | | | | | | | | | |
| | 48 | | | | | | | | | |

4. Discussion

Potential mechanisms of the anti-RF effect of SJZD were investigated and validated in this study. First, the *in vivo* efficacy test showed that SJZD could indeed improve renal function and reduce fibrosis in UUO-mice. Second, network pharmacology analysis provided in-depth insights into the anti-RF mechanism of SJZD, resulting in the following findings. Quercetin, Kaempferol, Naringenin and 7-Methoxy-2-methyl isoflavone were identified as the principal active components of anti-RF. Out of 187 intersection targets, PPI analysis successfully identified 3 key therapeutic targets (MAPK3, STAT3, and MYC) for the treatment of RF. Molecular docking results further demonstrated that Quercetin, Kaempferol and Naringenin could fit well into the active pocket of MAPK3 protein. Hence, it is

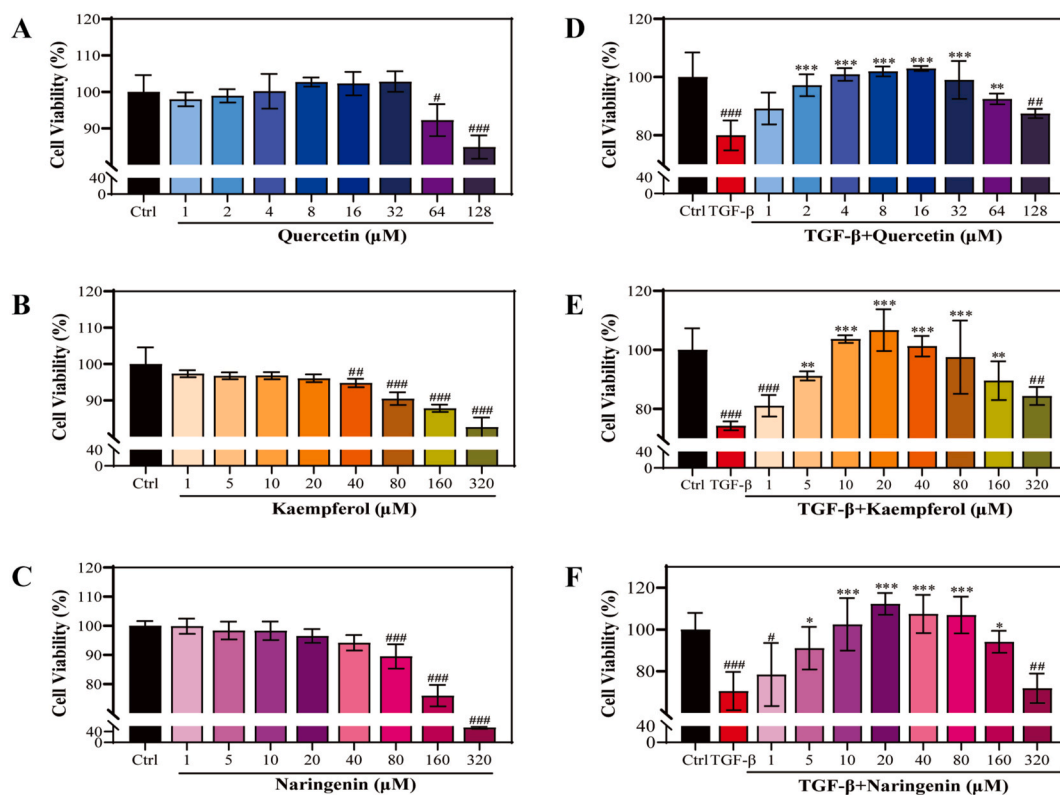


Fig. 9. Cell Viability. Cell viability with different concentrations of Quercetin (A), Kaempferol (B), and Naringenin (C). After induced with TGF- β , Cell viability with different concentrations of Quercetin (D), Kaempferol (E), and Naringenin (F). Data are represented as mean \pm SD. Superscript letters #, ## and ### denoted relative to control group $P < 0.05$, $P < 0.01$ and $P < 0.001$, respectively. Superscript letters *, ** and *** are denoted relative to model group $P < 0.05$, $P < 0.01$ and $P < 0.001$, respectively.

hypothesized that MAPK3 has the potential to be a valuable core target for treating RF. Finally, we demonstrated the potential of Quercetin, Kaempferol, and Naringenin attenuate TGF- β -induced fibrosis in HK-2 cells through *in vitro* experiments. Our findings indicate that these components and targets may represent a promising intervention for RF warranting further investigation.

Previous studies have shown that beneficial effects of bioflavonoids, such as Quercetin and Kaempferol, in ameliorating renal damage and fibrosis, particularly in patients with diabetic nephropathy [29,30]. The recruitment of inflammatory cells and release of cytokines and reactive oxygen species are often observed in the context of kidney damage, which ultimately results in the stimulation of fibroblasts and the production and accumulation of ECM proteins [31]. Recent research has also shown the capacity of Quercetin to regulate RF progression through its antioxidant activity and anti-inflammatory features [31]. In UUO-mice, it exhibits anti-inflammatory characteristics along with its capacity to mitigate oxidative stress and fibrosis, as well as inhibit the activation of AREG/EGFR signaling pathway [32]. Moreover, in the high glucose-induced rat model, it can also impede inflammation and oxidative stress mainly by controlling the miR-485-5p/YAP1 axis [33] and reduce RF by restraining the SIRT1/PINK1/mitophagy axis, controlling the PI3k/Akt pathway, and adjusting M1/M2 macrophage polarization [34–36]. It is noteworthy that the bioavailability of this compound can be significantly enhanced when rebuilt with nanoparticles, offering increased protection against kidney oxidative stress and the progression of RF in a gentamicin/adenine-induced rat model [37,38]. Additionally, Kaempferol plays a pivotal role in regulating oxidative stress and inhibiting the release of inflammation and cytokines through MAPK and NF-kappa B signaling pathways [39,40].

To gain further insight into the underlying mechanism of SJZD's anti-RF properties, GO and KEGG enrichment analyses were performed. GO analysis revealed a notable enrichment in biological functions such as Response to oxidative stress (GO:0006979), Response to lipopolysaccharide (GO:0032496), Response to decreased oxygen levels (GO:0036293) and other GO terms of Mitochondrial function. Hypoxic-reoxygenation injury increases the body's inflammatory response and mediates cell demise, ultimately resulting in renal tubular cell injury. Those pathological changes are predominantly related to the MAPK-ERK-CREB signaling pathway [41]. The progression of RF to ESRD is influenced by oxidative stress, therefore, the mitigation of oxidative stress can slow down the progression of RF to some extent [42]. Mitochondria are particularly sensitive to hypoxia and oxidative stress, and their impaired function leads to reduced energy supply to the kidney, which in turn damages renal tubular cells and exacerbates renal fibrosis development [43]. Asgharzadeh et al. also confirmed that prolonged exposure to lipopolysaccharide in rats causes an imbalance of oxidative stress, thus leading to the progression of RF [44]. KEGG data indicated that out of the 187 targets, 176 targets were major enriched in 180 signaling pathways. This finding highlights the therapeutic effect of SJZD on RF in different pathways. Among them,

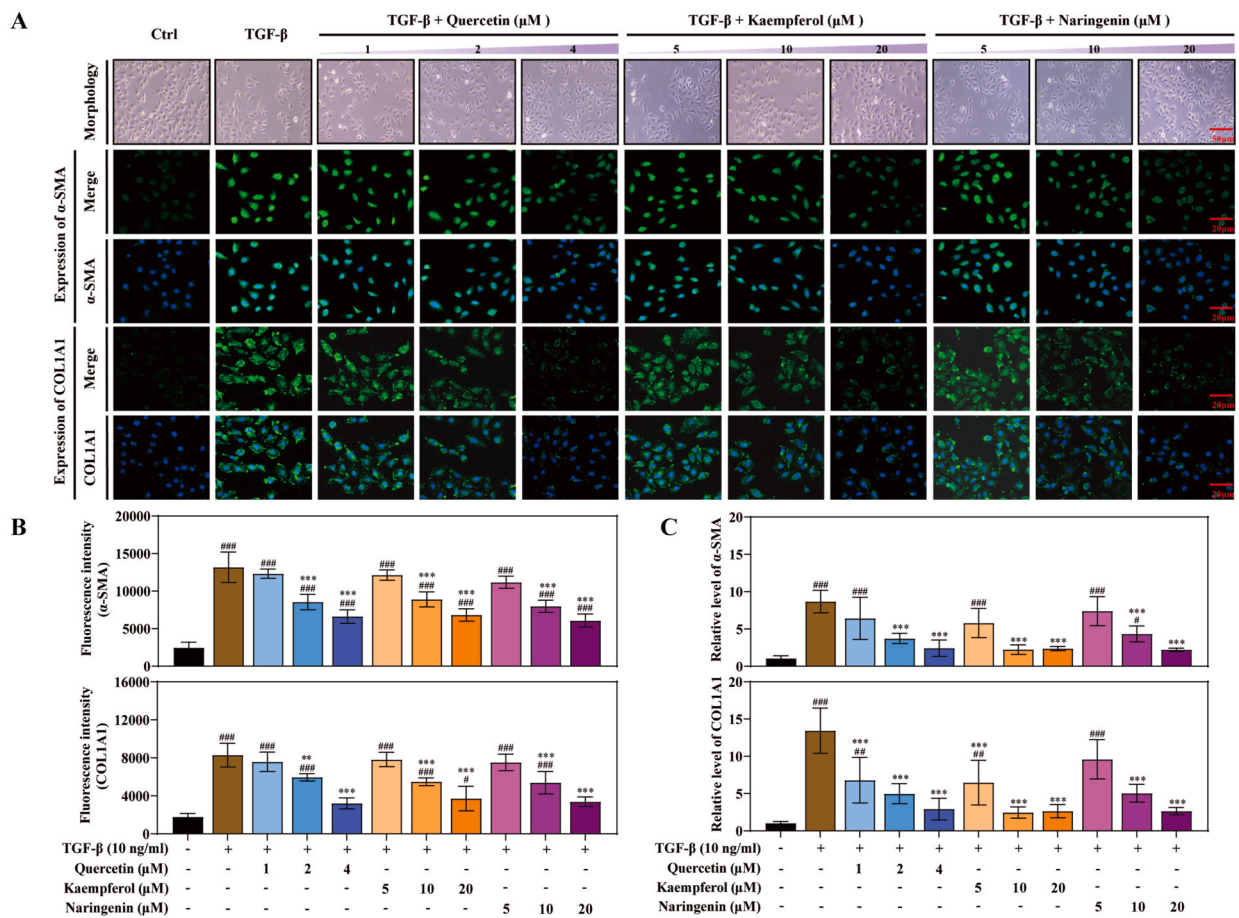


Fig. 10. (A) Cell morphology. Bar = 50 μ m. Immunofluorescence images for the protein expression of α -SMA, COL1A1. Bar = 20 μ m. (B) Statistical graph of protein expression levels of α -SMA and COL1A1. Data are represented as mean \pm SD. (C) Statistical graph for mRNA expression levels of α -SMA and COL1A1. Data are represented as mean \pm SD. Superscript letters #, ## and ### denoted relative to control group $P < 0.05$, $P < 0.01$ and $P < 0.001$, respectively. Superscript letters ** and *** are denoted relative to model group $P < 0.01$ and $P < 0.001$, respectively.

Lipid and atherosclerosis (hsa05417), AGE-RAGE signaling pathway in diabetic complications (hsa04933), Fluid shear stress and atherosclerosis (hsa05418), MAPK signaling pathway (hsa04010), etc. were considered to perform influential impact on the therapeutic benefits of SJZD on RF. Preliminary studies suggest that lipid metabolism disorders and atherosclerosis may mediate renal fibrosis through indirect pathways. The presence of foam cells loaded with lipids in the kidney and atherosclerotic plaques triggers inflammatory, oxidative, and endoplasmic reticulum stress responses, which facilitate the development of CKD [45]. Besides, an animal study showed that rats on a chronic high-fat diet accelerate oxidative stress leading to RF, mainly due to the presence of the NADPH oxidase MAPK/NF- κ B pathway, which promotes ox-LDL-induced collagen formation [46]. And AGE-RAGE signaling pathway has been implicated in both diabetic vascular calcification and fibrosis of the diabetic kidney, primarily driven by the activation of Nox-1 and TGF- β -induced fibrosis [47–49]. These results provide support for our claim that the above signaling pathways are integral to the SJZD-RF pathway and may play a major role in the anti-RF mechanism of SJZD.

In conjunction with the molecular docking results, MAPK3 emerges as a promising target for RF treatment with SJZD due to its significantly lower molecular docking binding energy (below -9.0 kcal/mol) with Quercetin, Kaempferol and Naringenin. MAPK3, commonly known as a member of MAPK (Mitogen-activated protein kinase) family, exerts a significant influence on cell proliferation, apoptosis, differentiation, and growth factor signaling [50,51]. Additionally, given that network pharmacology and molecular docking not only investigate the mechanism of the formula for treating diseases, but also explore the material basis of its function, we opted to verify core active ingredients through *in vitro* cell experiments rather than the entire formula. Therefore, Quercetin, Kaempferol and Naringenin were selected as the administration experimental group, with MAPK, α -SMA and collagen 1 (COL1A1) as the detection index for further *in vitro* experiments. Previous study has shown that inhibition of MAPK [52] is associated with a reduction in the expression of fibrosis markers and the progression of RF. α -SMA, as a hallmark of EMT, has been shown to stimulate the secretion of ECM and upregulates COL1A1, which is considered the initial event in fibrosis development. Our experimental results are consistent with this. In this study, we observed that HK-2 cells in the model group underwent a process known as EMT and ECM accumulation. Following treatment with different concentrations of Quercetin, Kaempferol and Naringenin, significant improvements were observed

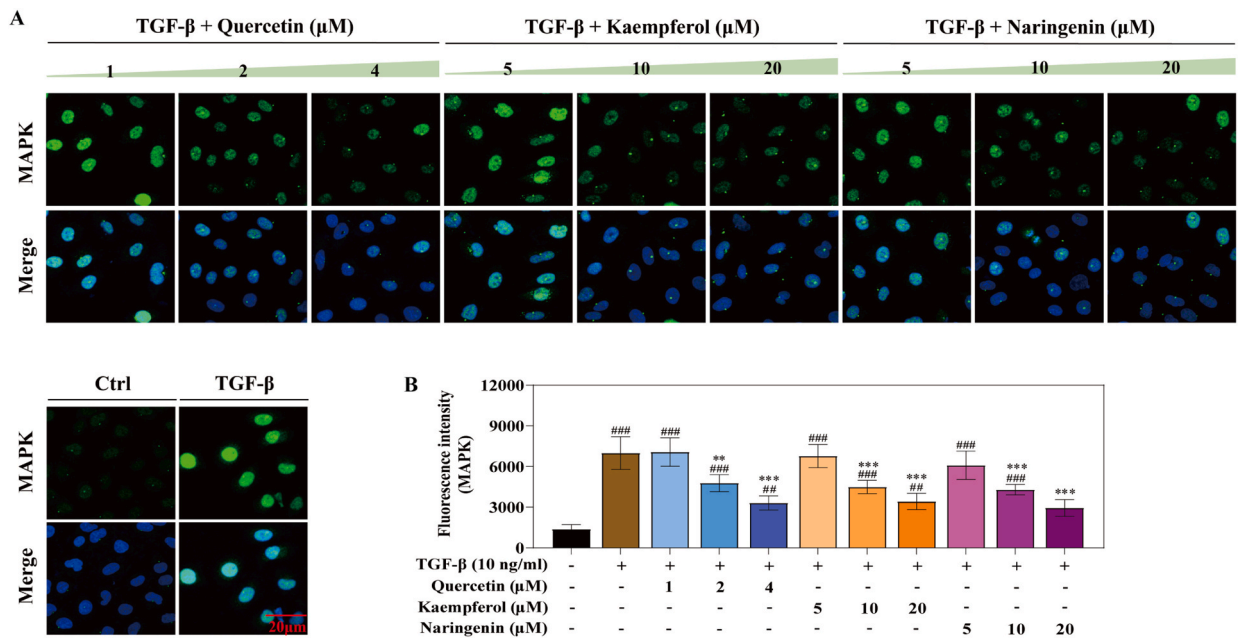


Fig. 11. (A) Representative immunofluorescence images for the protein expression of MAPK. Bar = 20 μm. (B) Statistical graph for protein expression levels of MAPK. Data are represented as mean ± SD. Superscript letters ^{##} and ^{###} denoted relative to control group $P < 0.01$ and $P < 0.001$, respectively. Superscript letters ^{**} and ^{***} are denoted relative to model group $P < 0.01$ and $P < 0.001$, respectively.

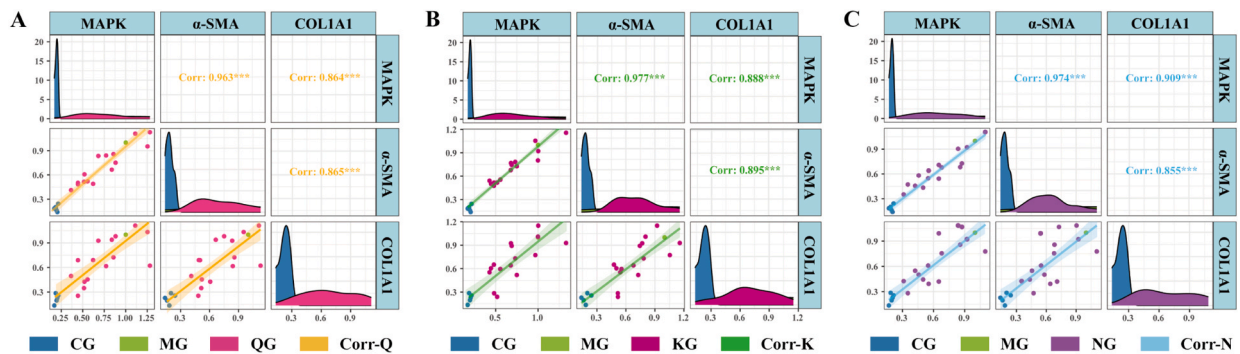


Fig. 12. Scatterplot matrix of within-group Pearson correlation analysis of Quercetin (A), Kaempferol (B) and Naringenin (C). Superscript letters ^{***} denoted relative to model group $P < 0.001$.

in these indicators including changes in cell expression of α-SMA, COL1A1, and MAPK proteins. Pearson correlation analysis further supported the significant correlation of these three indicators. Therefore, our hypothesis that Quercetin, kaempferol and Naringenin have the potential to impede ECM synthesis and reverse EMT, thereby improving the progression of RF, was validated. Nevertheless, it should be noted that the present study is not without its limitations. Firstly, the acquisition of active components is problematic, and there is no accurate prediction of the OB value for many components and low OB value does not necessarily indicate poor efficacy or few targets. Furthermore, the components that have been screened based on OB and DL values cannot confirm whether they can enter the bloodstream to reach target tissues and achieve the desired regulatory effects. Consequently, further experiments are required in subsequent stages to address these concerns.

5. Conclusion

In conclusion, this article explores the “multi-component, multi-target, multi-channel” characteristics of SJZD mediated RF therapy through network pharmacology, molecular docking and experimental validation. These findings lay the foundation for the clinical practice of SJZD in anti-RF.

Funding

The study described in this publication was partially funded by the Huai'an Science and Technology Bureau (HAB202211), the Scientific Research Project from Jiangsu Commission of Health of China (H2019062), Project of Science and Technology Development of Affiliated Hospital of Xuzhou Medical University (XYFM202248).

Ethics approval and consent to participation

The animal experimental procedures were conducted in compliance with the criteria established by the Animal Ethics Committee of Xuzhou Medical University (Ethics Approval Number: L20210226229).

Publication of clinical datasets

Not applicable.

Data availability statement

Data included in article/supplementary material/referenced in the article.

CRediT authorship contribution statement

Xinxin Yu: Writing – original draft, Visualization, Validation, Investigation, Data curation. **Xing Pu:** Writing – original draft, Visualization, Validation, Software, Data curation. **Yu Xi:** Writing – original draft, Visualization, Validation, Software, Data curation. **Xiang Li:** Visualization, Validation, Investigation, Data curation. **Wei Jiang:** Validation, Software, Investigation. **Xiaoling Chen:** Visualization, Validation, Investigation, Data curation. **Yong Xu:** Writing – review & editing, Methodology, Formal analysis, Data curation. **Juan Xie:** Writing – original draft, Software, Methodology, Formal analysis, Data curation. **Hailun Li:** Writing – review & editing, Supervision, Resources, Project administration, Methodology, Funding acquisition, Formal analysis. **Donghui Zheng:** Writing – review & editing, Supervision, Methodology, Formal analysis, Data curation.

Declaration of competing interest

The authors declare that they have no known competing financial interests or personal relationships that could have appeared to influence the work reported in this paper.

Acknowledgments

We are grateful to Professor Liang Jian of Guangzhou University of Chinese Medicine for his experimental assistance.

Appendix A. Supplementary data

Supplementary data to this article can be found online at <https://doi.org/10.1016/j.heliyon.2024.e35489>.

References

- [1] X.Y. Liu, X.B. Zhang, Y.F. Zhao, K. Qu, X.Y. Yu, Research progress of Chinese herbal medicine intervention in renal interstitial fibrosis, *Front. Pharmacol.* 13 (2022) 900491, <https://doi.org/10.3389/fphar.2022.900491>.
- [2] X. Zhao, Y. Kong, B. Liang, et al., Mechanosensitive Piezo1 channels mediate renal fibrosis, *JCI Insight* 7 (7) (2022) e152330, <https://doi.org/10.1172/jci.insight.152330>.
- [3] GBD Chronic Kidney Disease Collaboration, Global, regional, and national burden of chronic kidney disease, 1990–2017: a systematic analysis for the Global Burden of Disease Study 2017, *Lancet* 395 (10225) (2020) 709–733, [https://doi.org/10.1016/S0140-6736\(20\)30045-3](https://doi.org/10.1016/S0140-6736(20)30045-3).
- [4] P. Ma, Y. Peng, L. Zhao, F. Liu, X. Li, Differential effect of polysaccharide and nonpolysaccharide components in Sijunzi decoction on spleen deficiency syndrome and their mechanisms, *Phytomedicine* 93 (2021) 153790, <https://doi.org/10.1016/j.phymed.2021.153790>.
- [5] P. Lyu, J. Bao, C. Mou, Exploration on the origin and clinical significance of master-slave relationship between spleen and kidney by Mou Chong-lin, *China. J. Tradit. Chinese. Med. Pharm.* 35 (2020) 3051–3054.
- [6] Z. Liu, Y. Wei, B. Wu, Spleen and kidney related theory and its application, *J. Tradit. Chin. Med.* 53 (2012) 1351–1364.
- [7] D. Kiefer, T. Pantuso, Panax ginseng, *Am. Fam. Physician* 68 (8) (2003) 1539–1542.
- [8] R. Yang, B.C. Yuan, Y.S. Ma, S. Zhou, Y. Liu, The anti-inflammatory activity of licorice, a widely used Chinese herb, *Pharm. Biol.* 55 (1) (2017) 5–18, <https://doi.org/10.1080/13880209.2016.1225775>.
- [9] L. Yang, H. Yu, A. Hou, et al., A review of the ethnopharmacology, phytochemistry, pharmacology, application, quality control, processing, toxicology, and pharmacokinetics of the dried rhizome of *Atractylodes macrocephala*, *Front. Pharmacol.* 12 (2021) 727154, <https://doi.org/10.3389/fphar.2021.727154>.
- [10] M. Fan, X. Lan, Q. Wang, et al., Renal function protection and the mechanism of ginsenosides: current progress and future perspectives, *Front. Pharmacol.* 14 (2023) 1070738, <https://doi.org/10.3389/fphar.2023.1070738>.

- [11] M. Wang, D.Q. Chen, L. Chen, et al., Novel RAS inhibitors poricoic acid ZG and poricoic acid ZH attenuate renal fibrosis via a Wnt/ β -catenin pathway and targeted phosphorylation of Smad3 signaling, *J. Agric. Food Chem.* 66 (8) (2018) 1828–1842, <https://doi.org/10.1021/acs.jafc.8b00099>.
- [12] Y. Zhou, Y. Zhou, L. Gao, P. Xia, et al., Glycyrrhetic acid protects renal tubular cells against oxidative injury via reciprocal regulation of JNK-connexin 43-thioredoxin 1 signaling, *Front. Pharmacol.* 12 (2021) 619567, <https://doi.org/10.3389/fphar.2021.619567>.
- [13] X. Hu, S. Zhu, Z. Gao, Effect of Sijunzi Decoction combined with western medicine in the treatment of chronic kidney disease of stage 3-5 with kidney deficiency and dampness turbidity syndrome and its influence on renal function and calcium and phosphorus metabolism levels, *Hainan. Med. J.* 33 (2022) 1537–1540.
- [14] da C. Hao, P.G. Xiao, Network pharmacology: a rosetta stone for traditional Chinese medicine, *Drug Dev. Res.* 75 (5) (2014) 299–312, <https://doi.org/10.1002/ddr.21214>.
- [15] C. Nogales, Z.M. Mamdouh, M. List, C. Kiel, A.I. Casas, H.H.H.W. Schmidt, Network pharmacology: curing causal mechanisms instead of treating symptoms, *Trends Pharmacol. Sci.* 43 (2) (2022) 136–150, <https://doi.org/10.1016/j.tips.2021.11.004>.
- [16] H. Xu, J. Wu, S. Wang, et al., Network pharmacology and *in vivo* experiments reveal the pharmacological effects and molecular mechanisms of Simiao Powder in prevention and treatment for gout, *BMC Complement Med. Ther.* 22 (1) (2022) e152, <https://doi.org/10.1186/s12906-022-03622-0>.
- [17] X. Li, S. Wei, S. Niu, et al., Network pharmacology prediction and molecular docking-based strategy to explore the potential mechanism of Huanglian Jiedu Decoction against sepsis, *Comput. Biol. Med.* 144 (2022) e105389, <https://doi.org/10.1016/j.compbiomed.2022.105389>.
- [18] S. He, T. Wang, C. Shi, Z. Wang, X. Fu, Network pharmacology-based approach to understand the effect and mechanism of Danshen against anemia, *J. Ethnopharmacol.* 282 (2022) 114615, <https://doi.org/10.1016/j.jep.2021.114615>.
- [19] S. Forli, R. Huey, M.E. Pique, M.F. Sanner, D.S. Goodsell, A.J. Olson, Computational protein-ligand docking and virtual drug screening with the AutoDock suite, *Nat. Protoc.* 11 (5) (2016) 905–919, <https://doi.org/10.1038/nprot.2016.051>.
- [20] J. Liu, J. Liu, X. Tong, et al., Network pharmacology prediction and molecular docking-based strategy to discover the potential pharmacological mechanism of Huai Hua San against ulcerative colitis, *Drug Des. Dev. Ther.* 15 (2021) 3255–3276, <https://doi.org/10.2147/DDDT.S319786>.
- [21] H. Li, Z. Yan, Q. Xiong, et al., Renoprotective effect and mechanism of polysaccharide from *Polyporus umbellatus* sclerotia on renal fibrosis, *Carbohydr. Polym.* 212 (2019) 1–10, <https://doi.org/10.1016/j.carbpol.2019.02.026>.
- [22] H. Li, X. Pu, Y. Lin, et al., Sijunzi decoction alleviates inflammation and intestinal epithelial barrier damage and modulates the gut microbiota in ulcerative colitis mice, *Front. Pharmacol.* 15 (2024) 1360972, <https://doi.org/10.3389/fphar.2024.1360972>.
- [23] Y. Shi, L. Zhou, G. Zheng, et al., Therapeutic mechanism exploration of polysaccharides from *Dendrobium officinale* on unilateral ureteral obstruction operation-induced renal fibrosis based on improving oxidative stress injury mediated by AhR/NOX4 pathway, *Int. J. Biol. Macromol.* 253 (2023) e126920, <https://doi.org/10.1016/j.ijbiomac.2023.126920>.
- [24] J. Ru, P. Li, J. Wang, et al., TC MSP: a database of systems pharmacology for drug discovery from herbal medicines, *J. Cheminf.* 6 (2014) 13, <https://doi.org/10.1186/1758-2946-6-13>. Published 2014 Apr 16.
- [25] S. Li, B. Zhang, Traditional Chinese medicine network pharmacology: theory, methodology and application, *Chin. J. Nat. Med.* 11 (2) (2013) 110–120.
- [26] Y. Tang, M. Li, J. Wang, Y. Pan, F.X. Wu, CytoNCA: a cytoscape plugin for centrality analysis and evaluation of protein interaction networks, *Biosystems* 127 (2015) 67–72, <https://doi.org/10.1016/j.biosystems.2014.11.005>.
- [27] X. Zhao, Z.P. Liu, Analysis of topological parameters of complex disease genes reveals the importance of location in a biomolecular network, *Genes* 10 (2) (2019) 143, <https://doi.org/10.3390/genes10020143>.
- [28] P. Schober, C. Boer, L.A. Schwarte, Correlation coefficients: appropriate use and interpretation, *Anesth. Analg.* 126 (5) (2018) 1763–1768, <https://doi.org/10.1213/ANE.0000000000002864>.
- [29] Q. Lu, X.J. Ji, Y.X. Zhou, et al., Quercetin inhibits the mTORC1/p70S6K signaling-mediated renal tubular epithelial-mesenchymal transition and renal fibrosis in diabetic nephropathy, *Pharmacol. Res.* 99 (2015) 237–247, <https://doi.org/10.1016/j.phrs.2015.06.006>.
- [30] D. Sharma, R. Kumar Tekade, K. Kalia, Kaempferol in ameliorating diabetes-induced fibrosis and renal damage: an *in vitro* and *in vivo* study in diabetic nephropathy mice model, *Phytomedicine* 76 (2020) 153235, <https://doi.org/10.1016/j.phymed.2020.153235>.
- [31] Y.Q. Chen, H.Y. Chen, Q.Q. Tang, et al., Protective effect of quercetin on kidney diseases: from chemistry to herbal medicines, *Front. Pharmacol.* 13 (2022) 968226, <https://doi.org/10.3389/fphar.2022.968226>.
- [32] Q. Wang, F. Wang, X. Li, Z. Ma, D. Jiang, Quercetin inhibits the amphiregulin/EGFR signaling-mediated renal tubular epithelial-mesenchymal transition and renal fibrosis in obstructive nephropathy, *Phytother. Res.* 37 (1) (2023) 111–123, <https://doi.org/10.1002/ptr.7599>.
- [33] H. Wan, Y. Wang, Q. Pan, et al., Quercetin attenuates the proliferation, inflammation, and oxidative stress of high glucose-induced human mesangial cells by regulating the miR-485-5p/YAP1 pathway, *Int. J. Immunopathol. Pharmacol.* 36 (2022) 20587384211066440, <https://doi.org/10.1177/20587384211066440>.
- [34] T. Liu, Q. Yang, X. Zhang, et al., Quercetin alleviates kidney fibrosis by reducing renal tubular epithelial cell senescence through the SIRT1/PINK1/mitophagy axis, *Life Sci.* 257 (2020) 118116, <https://doi.org/10.1016/j.lfs.2020.118116>.
- [35] H. Lu, L. Wu, L. Liu, et al., Quercetin ameliorates kidney injury and fibrosis by modulating M1/M2 macrophage polarization, *Biochem. Pharmacol.* 154 (2018) 203–212, <https://doi.org/10.1016/j.bcp.2018.05.007>.
- [36] H. Tu, D. Ma, Y. Luo, et al., Quercetin alleviates chronic renal failure by targeting the PI3k/Akt pathway, *Bioengineered* 12 (1) (2021) 6538–6558, <https://doi.org/10.1080/21655979.2021.1973877>.
- [37] A. Rahdar, P. Hasanein, M. Bilal, H. Beyzaei, G.Z. Kyzas, Quercetin-loaded F127 nanomicelles: antioxidant activity and protection against renal injury induced by gentamicin in rats, *Life Sci.* 276 (2021) 119420, <https://doi.org/10.1016/j.lfs.2021.119420>.
- [38] E.A. Sánchez-Jaramillo, L.E. Gasca-Lozano, J.M. Vera-Cruz, et al., Nanoparticles formulation improves the antifibrogenic effect of quercetin on an adenine-induced model of chronic kidney disease, *Int. J. Mol. Sci.* 23 (10) (2022) 5392, <https://doi.org/10.3390/ijms23105392>.
- [39] A.S. Alshetri, A.F. El-Kott, A.E. El-Kenawy, et al., The ameliorative effect of kaempferol against CdCl₂-mediated renal damage entails activation of Nrf2 and inhibition of NF- κ B, *Environ. Sci. Pollut. Res. Int.* 29 (38) (2022) 57591–57602, <https://doi.org/10.1007/s11356-022-19876-7>.
- [40] Q. Wu, J. Chen, X. Zheng, et al., Kaempferol attenuates doxorubicin-induced renal tubular injury by inhibiting ROS/ASK1-mediated activation of the MAPK signaling pathway, *Biomed. Pharmacother.* 157 (2023) 114087, <https://doi.org/10.1016/j.biopha.2022.114087>.
- [41] Q. Dong, Y. Jie, J. Ma, C. Li, T. Xin, D. Yang, Renal tubular cell death and inflammation response are regulated by the MAPK-ERK-CREB signaling pathway under hypoxia-reoxygenation injury, *J. Recept. Signal Transduct. Res.* 39 (5–6) (2019) 383–391, <https://doi.org/10.1080/10799893.2019.1698050>.
- [42] H. Su, C. Wan, A. Song, Y. Qiu, W. Xiong, C. Zhang, Oxidative stress and renal fibrosis: mechanisms and therapies, *Adv. Exp. Med. Biol.* 1165 (2019) 585–604, https://doi.org/10.1007/978-981-13-8871-2_29.
- [43] M. Bai, M. Wu, M. Jiang, J. He, X. Deng, S. Xu, J. Fan, M. Miao, T. Wang, Y. Li, X. Yu, L. Wang, Y. Zhang, S. Huang, L. Yang, Z. Jia, A. Zhang, LONP1 targets HMGCs2 to protect mitochondrial function and attenuate chronic kidney disease, *EMBO Mol. Med.* 15 (2) (2023) e16581, <https://doi.org/10.15252/emmm.202216581>.
- [44] F. Asgharzadeh, R. Bargi, M. Hosseini, M. Farzadnia, M. Khazaei, Cardiac and renal fibrosis and oxidative stress balance in lipopolysaccharide-induced inflammation in male rats, *ARYA Atheroscler* 14 (2) (2018) 71–77, <https://doi.org/10.22122/arya.v14i2.1550>.
- [45] X.G. Du, X.Z. Ruan, Lipid metabolism disorder and renal fibrosis, *Adv. Exp. Med. Biol.* 1165 (2019) 525–541, https://doi.org/10.1007/978-981-13-8871-2_26.
- [46] Y. Dai, P. Palade, X. Wang, et al., High fat diet causes renal fibrosis in LDLR-null mice through MAPK-NF- κ B pathway mediated by Ox-LDL, *J. Cardiovasc. Pharmacol.* 63 (2) (2014) 158–166, <https://doi.org/10.1097/FJC.0000000000000035>.
- [47] A.M. Kay, C.L. Simpson, J.A. Stewart Jr., The role of AGE/RAGE signaling in diabetes-mediated vascular calcification, *J. Diabetes Res.* 2016 (2016) 6809703, <https://doi.org/10.1155/2016/6809703>.
- [48] N. Pathomthongtawechai, S. Chutipongtanate, AGE/RAGE signaling-mediated endoplasmic reticulum stress and future prospects in non-coding RNA therapeutics for diabetic nephropathy, *Biomed. Pharmacother.* 131 (2020) 110655, <https://doi.org/10.1016/j.biopha.2020.110655>.
- [49] I. Tuleta, N.G. Frangogiannis, Diabetic fibrosis, *Biochim. Biophys. Acta, Mol. Basis Dis.* 1867 (4) (2021) 166044, <https://doi.org/10.1016/j.bbadis.2020.166044>.

- [50] K. Kurtzeborn, H.N. Kwon, S. Kuure, MAPK/ERK signaling in regulation of renal differentiation, *Int. J. Mol. Sci.* 20 (7) (2019) 1779, <https://doi.org/10.3390/ijms20071779>.
- [51] A. Safa, A. Abak, H. Shoorei, M. Taheri, S. Ghafouri-Fard, MicroRNAs as regulators of ERK/MAPK pathway: a comprehensive review, *Biomed. Pharmacother.* 132 (2020) 110853, <https://doi.org/10.1016/j.biopha.2020.110853>.
- [52] X.Q. Geng, A. Ma, J.Z. He, et al., Ganoderic acid hinders renal fibrosis via suppressing the TGF- β /Smad and MAPK signaling pathways, *Acta Pharmacol. Sin.* 41 (5) (2020) 670–677, <https://doi.org/10.1038/s41401-019-0324>.